Oncogene
https://doi.org/10.1038/s41388-020-1204-9

BRIEF COMMUNICATION

Genetic basis for iMCD-TAFRO

Akihide Yoshimi[1] · Tanya M. Trippett[2] · Nan Zhang[3,11] · Xueyan Chen[4] · Alexander V. Penson[1,5] · Maria E. Arcila[6,7] · Janine Pichardo[6] · Jeeyeon Baik[6] · Allison Sigler[6] · Hironori Harada[8] · David C. Fajgenbaum[9] · Ahmet Dogan[6] · Omar Abdel-Wahab[1,10] · Wenbin Xiao[1,6]

Received: 9 November 2019 / Revised: 20 January 2020 / Accepted: 30 January 2020

Abstract

TAFRO syndrome, a clinical subtype of idiopathic multicentric Castleman disease (iMCD), consists of a constellation of symptoms/signs including thrombocytopenia, anasarca, fever, reticulin fibrosis/renal dysfunction, and organomegaly. The etiology of iMCD-TAFRO and the basis for cytokine hypersecretion commonly seen in iMCD-TAFRO patients has not been elucidated. Here, we identified a somatic *MEK2*^{P128L} mutation and a germline *RUNX1*^{G60C} mutation in two patients with iMCD-TAFRO, respectively. The *MEK2*^{P128L} mutation, which has been identified previously in solid tumor and histiocytosis patients, caused hyperactivated MAP kinase signaling, conferred IL-3 hypersensitivity and sensitized the cells to various MEK inhibitors. The *RUNX1*^{G60C} mutation abolished the transcriptional activity of wild-type RUNX1 and functioned as a dominant negative form of RUNX1, resulting in enhanced self-renewal activity in hematopoietic stem/progenitor cells. Interestingly, ERK was heavily activated in both patients, highlighting a potential role for activation of MAPK signaling in iMCD-TAFRO pathogenesis and a rationale for exploring inhibition of the MAPK pathway as a therapy for iMCD-TAFRO. Moreover, these data suggest that iMCD-TAFRO might share pathogenetic features with clonal inflammatory disorders bearing *MEK* and *RUNX1* mutations such as histiocytoses and myeloid neoplasms.

Introduction

TAFRO syndrome is a clinical subtype of idiopathic multicentric Castleman disease (iMCD) characterized by thrombocytopenia, anasarca, fever, reticulin fibrosis/renal dysfunction, and organomegaly [1, 2]. iMCD-TAFRO can occur in individuals of all ages, with a median age of 50 and a slight predilection for male gender [3]. Similar to other cases of iMCD, iMCD-TAFRO patients often present with elevated serum cytokines and chemokines including IL-6, IP-10, MDC, and CXCL13 [4, 5]. The etiology of iMCD-TAFRO and the basis for cytokine hypersecretion has not been elucidated, although germline and somatic genetic alterations have been proposed to underlie iMCD-TAFRO [6]. Here, we

These authors contributed equally: Omar Abdel-Wahab, Wenbin Xiao

Supplementary information The online version of this article (https://doi.org/10.1038/s41388-020-1204-9) contains supplementary material, which is available to authorized users.

✉ Wenbin Xiao
xiaow@mskcc.org

1 Human Oncology and Pathogenesis Program, Memorial Sloan Kettering Cancer Center, New York, NY 10065, USA

2 Department of Pediatrics, Memorial Sloan Kettering Cancer Center, New York, NY 10065, USA

3 Department of Pathology, Buffalo General Medical Center, SUNY at Buffalo, Buffalo, NY 14206, USA

4 Department of Laboratory Medicine, University of Washington, Seattle, WA 98109, USA

5 Department of Epidemiology and Biostatistics, Memorial Sloan Kettering Cancer Center, New York, NY 10065, USA

6 Department of Pathology, Hematopathology service, Memorial Sloan Kettering Cancer Center, New York, NY 10065, USA

7 Department of Pathology, Diagnostic Molecular laboratory, Memorial Sloan Kettering Cancer Center, New York, NY 10065, USA

8 Laboratory of Oncology, School of Life Sciences, Tokyo University of Pharmacy and Life Sciences, Hachioji, Tokyo 192-0392, Japan

9 Castleman Disease Collaborative Network, Philadelphia, PA, USA

10 Department of Medicine, Leukemia Service, Memorial Sloan Kettering Cancer Center, New York, NY 10065, USA

11 Present address: Department of Pathology, Rochester General Hospital, Rochester, NY 14621, USA

Published online: 12 February 2020

report the identification and functional characterization of a somatic *MEK2* mutation and a germline *RUNX1* mutation in two iMCD-TAFRO patients, respectively.

Results and discussion

Identification of somatic *MAP2K2* (*MEK2*) mutation and germline *RUNX1* mutation in patients with iMCD-TAFRO

Clinical information was provided by treating physicians and extracted from electronic medical records. Studies were approved by the Institutional Review Boards of Memorial Sloan Kettering Cancer Center. Three patients (male, 32-year-old, 3-year-old, and 20-year-old) presented with typical signs and symptoms of iMCD-TAFRO including fever, anasarca, leukocytosis, anemia, thrombocytopenia, renal insufficiency, hepatosplenomegaly, diffuse lymphadenopathy, and evidence of systemic inflammation with elevated ESR, CRP, and IL-6 levels (Table 1). Evaluation for autoantibodies and viruses (HHV-8, EBV) were negative. Lymph node excisional biopsies (neck and inguinal nodes, respectively) were compatible with iMCD-TAFRO (Fig. 1a, Supplementary Fig. S1a) [7]. Bone marrow (BM) biopsies revealed moderately increased megakaryocytes with occasional megakaryocytic emperipolesis and increased reticulin fibrosis. Flow cytometric analyses of nodal and marrow specimens were negative for lymphoma or leukemia. The overall findings were compatible with iMCD-TAFRO. All three patients were treated with high-dose steroids and anti-IL-6 antibodies (two Tocilizumab and one Siltuximab) and obtained complete remission of symptoms including lymphadenopathy (Fig. 1b, c).

In order to evaluate for potential genetic alterations underlying iMCD-TAFRO, the coding region of ~500 genes implicated in cancer was sequenced by a next generation sequencing platform (MSK-IMPACT) on the lymph node biopsy tissue from the three patients. Several germline variants of unclear significance were detected (Table 2). Among these variants, mutations in *MEK2* and *RUNX1* are commonly identified in a variety of cancers and were predicted to be damaging by both SIFT and Polyphen-2 programs. In addition, sequencing of the lymph node from Patient 1 identified a *MAP2K2* (*MEK2*) p.P128L mutation with a variant allele frequency (VAF) of 10%, which was absent from the patient's BM, indicative of a somatic mutation. Although the function of this specific mutant has not been characterized previously, it is recurrent across several cancer types and predicted to activate MAPK signaling (Fig. 1d). Sequencing of Patient 2 identified a *RUNX1* p.G60C variant with similarly high VAF across nodal (48%), marrow (49%), and nail DNA (49%), indicative of a germline variant. RUNX1 p.G60C, located at the N-terminus of the Runt DNA binding domain (Fig. 1e), has

Table 1 Clinicopathologic features of iMCD-TAFRO patients.

	Patient 1	Patient 2	Patient 3
Age (years)	32	3	20
Sex	M	M	M
Fever	Yes	Yes	Yes
Anasarca	Large pleural effusion and ascites	Pleural effusion, ascites, pericardial effusion	Pleural effusion, ascites, pericardial effusion
Hb (g/dL)	10.8	7.8	5.1
PLT ($\times 10^3$/dL)	32	14	100
ALP (U/L)	Not available	108	300
LDH (U/L)	Not available	481	409
Viral workup (EBV/HHV-8/adenovirus/rhinovirus)	Negative	Negative	Negative
Autoantibodies	Negative	Negative	Negative
Renal insufficiency	Yes	Yes	Yes (Hemodialysis)
Organomegaly	Yes	Yes	Yes
Lymphadenopathy	Diffuse	Diffuse	Diffuse
Castleman like changes in node	Yes	Yes	Yes
Flow cytometry in node	Negative	Negative	Negative
Bone marrow atypical megakaryocytes	Yes	Yes	Yes
Bone marrow fibrosis	Yes (MF1-2/3)	Yes (MF1/3)	Yes (MF1-2/3)
Bone marrow flow cytometry	Negative	Negative	Negative
JAK2/MPL/CALR mutations	Negative	Negative	Negative
Serum IL-6 level	43.6 pg/mL	Significantly increased	138.2 pg/mL
Anti-IL-6 treatment	Tocilizumab	Tocilizumab	Siltuximab
Steroids treatment	Yes	Yes	Yes
Follow-up	Recovered, but relapsed	Recovered, no relapse for 3 years	Recovered

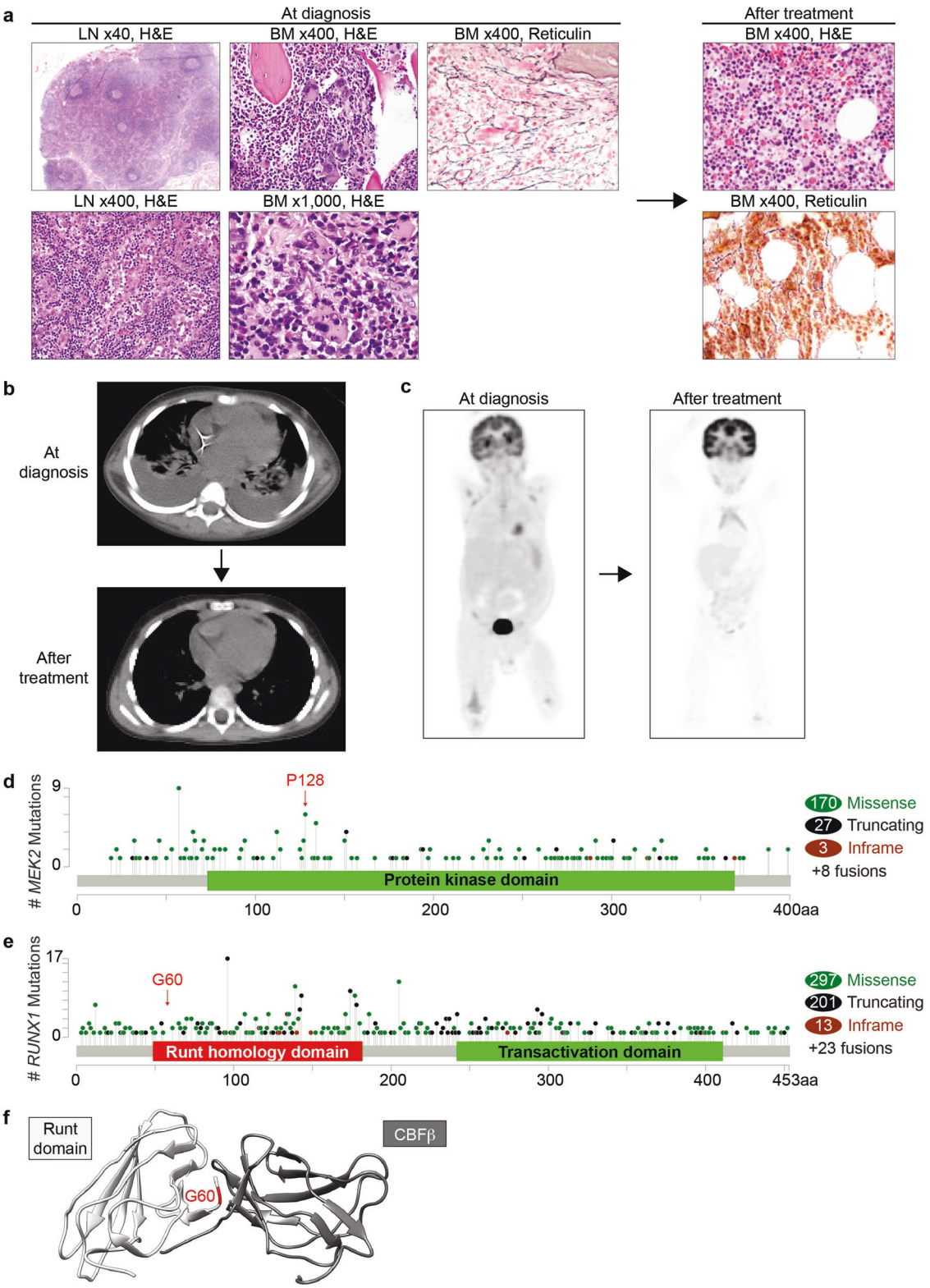

not been previously reported but is structurally predicted to affect the heterodimerization of RUNX1 with CBFβ, which is essential for RUNX1 function (Fig. 1f). We also examined for possible fusions by targeted next generation RNA sequencing (199-gene Archer panel) in all three patients but no in-frame fusions were detected. Based on these observations, we chose *MEK2* and *RUNX1* variants for further functional studies, although we cannot completely exclude the possibility that the other variants (such as *RARA* and *SETD2* variants in patient 3) could also be pathogenic.

◀ **Fig. 1 Clinical presentation and genetic features of patients with iMCD-TAFRO. a** Hematoxylin & eosin (H&E) and reticulin stain of a lymph node (LN) and bone marrow (BM) at diagnosis and after treatment (Patient 2; magnifications are indicated). Representative plain CT (**b**) and PET scan (**c**) images of Patient 2 at diagnosis and after treatment. Lollipop graphs showing frequencies of mutations in *MEK2* (**d**) and *RUNX1* (**e**) across cancers. Figures were made based on the cBioPortal data of 42,049 samples derived from TCGA PanCancer Atlas Studies and curated set of non-redundant studies (158 studies in total) and the location of mutations that were identified in Patients 1 and 2 are highlighted. Mutations affecting MEK2^{P128} were identified in 3 bladder carcinoma, 1 melanoma, and 1 pancreatic ductal adenocarcinoma. **f** Structure of WT Runt homology domain (white) and CBFβ (gray) with RUNX1^{G60C} position highlighted in red. Figure was made based on PDB ID: 1E50.

Pathogenetic roles of mutant MEK2 and mutant RUNX1

To determine the functional impact of the somatic *MEK2* mutation, we expressed wild-type (WT) MEK2 and MEK2^{P128L} into 32D cells and examined the effects on IL-3 dependent growth and downstream signaling. Although MEK2^{P128L} did not confer cytokine independence, 32D cells expressing MEK2^{P128L} had robust growth at very low IL-3 concentrations in which control cells could not survive (Fig. 2a, b), demonstrating cytokine hypersensitivity conferred by MEK2^{P128L}. Accordingly, MEK2^{P128L} enhanced phosphorylation of MEK1/2 and downstream ERK1/2 constitutively and after IL-3 stimulation (Fig. 2c). Although BaseScope technology detected MEK2^{P128L} mRNA in a minor subset of cells in the nodal biopsy (Supplementary Fig. S1b), levels of phospho-ERK1/2 by immunohistochemistry were increased in the biopsy tissue and corresponded to histiocytes and/or follicular dendritic cells (Fig. 2d) while lymphocytes had no detectable phospho-ERK. Consistent with these observations, 32D cells expressing MEK2^{P128L} were sensitive to various MEK inhibitors (Trametinib, Selumetinib, and U0126) (Fig. 2e, Supplementary Fig. S2a, b), demonstrating suppressed cell growth and ERK activation in a dose-dependent manner (Fig. 2f, g, Supplementary Fig. S2c–e). Interestingly, phospho-ERK expressing cells were also increased in patient 2 with the *RUNX1*^{G60C} mutation (Fig. 2d). These results suggest that the MAP kinase pathway might be commonly activated in iMCD-TAFRO and that inhibition of MAPK pathway could be a potential therapeutic strategy for iMCD-TAFRO.

Unlike MEK2^{P128L}, expression of RUNX1^{G60C} did not affect the growth of 32D cells (data not shown). However, given the location of this mutation within the RUNT DNA binding domain, we investigated the effect of mutant RUNX1^{G60C} on RUNX1 transcriptional activity. Using a luciferase reporter assay for a well-known RUNX1 target gene, M-CSFR, RUNX1^{WT} clearly induced RUNX1 transcriptional activity, an effect completely abolished in the presence of RUNX1^{G60C} (Fig. 2h). Furthermore, RUNX1^{G60C} suppressed the activity of its WT counterpart, suggesting a dominant negative effect (Fig. 2i, Supplementary Fig. S2f). As patients with germline *RUNX1* mutations are predisposed to myeloid neoplasms, we transduced RUNX1^{G60C} into mouse BM progenitor cells and performed colony-forming assay. MEK2^{P128L} had no effect on number or types of primary colonies and showed mildly increased colonies at second passage with no impact on serial replating capacity, suggesting that MEK2^{P128L} does not affect self-renewal capacity. In contrast, RUNX1^{G60C} significantly enhanced self-renewal capacity of BM progenitors to the same extent as the RUNX1/RUNX1T1 fusion (Fig. 2j, k, Supplementary Fig. S2g). Somatic *MEK2* mutations occur in histiocytoses [8] while somatic *RUNX1* mutations occur in myeloid neoplasms and are associated with predisposition to myeloid neoplasms when present in the germline [9, 10]. These results suggest that iMCD-TAFRO might be related to a wider spectrum of diseases that converge on the same constellation associated with cytokine/chemokine hypersecretion. In fact, expression of both MEK2^{P128L} and RUNX1^{G60C} induced overproduction of some of the key cytokines/chemokines known to be elevated in iMCD-TAFRO including IL-6, IP-10, and MDC [4, 5] (Supplementary Fig. S3a–c).

The data above identify pathogenic genetic variants in two out of three subjects studied with iMCD-TAFRO. Although a *DNMT3A* mutation was previously reported in an iMCD-TAFRO patient [11], the causative relationship of this mutation to iMCD-TAFRO is uncertain as *DNMT3A* is frequently mutated in clonal hematopoiesis [12, 13]. Another study reported a germline *FASL* mutation in a family with unicentric Castleman disease and iMCD [14]. However, germline *FASL* mutations are nearly pathognomonic for autoimmune lymphoproliferative syndrome, a condition that can resemble Castleman disease [15]. Instead, here we identified germline and somatic mutations in iMCD-TAFRO patients which have been implicated in clonal hematopoietic disorders and we demonstrate impact on gene function. These results suggest that iMCD-TAFRO might share pathogenetic features with these other clonal inflammatory disorders.

Materials and methods

Patient samples

Tissues were obtained from three patients with iMCD-TAFRO. Clinical information was provided by treating physicians. Studies were approved by the Institutional Review Boards of Memorial Sloan Kettering Cancer Center (under MSK IRB protocol X17-025). Written informed consent was obtained from the three participants.

Table 2 Variants detected in iMCD-TAFRO patients.

	Gene	Protein change	Allele Freq.	Chr.	Start pos.	End pos.	Ref.	Var	SIFT prediction	Polyphen-2 prediction
Patient 1	*MAP2K2 (MEK2)*	P128L	0.10	19	4,110,574	4,110,574	G	A	Damaging	Probably damaging
	AR	A646D	0.99	X	66,931,295	66,931,295	C	A	Tolerated	Benign
	TCF3	N347T	0.49	19	1,621,020	1,621,020	T	G	Tolerated	Probably damaging
	ARID2	T1193A	0.46	12	46,245,483	46,245,483	A	G	Tolerated	Benign
Patient 2	*KMT2B (MLL4)*	E373del	0.40	19	36,211,355	36,211,357	AAG	A	–	–
	MPEG1	L221I	0.50	11	58,979,678	58,979,678	G	T	Tolerated	Benign
	RUNX1	G60C	0.48	21	36,259,232	36,259,232	C	A	Damaging	Probably damaging
Patient 3	*EGFR*	H145R	0.46	7	55,214,308	55,214,308	A	G	Tolerated	Benign
	EPHA3	S662T	0.52	3	89,462,392	89,462,392	T	G	Tolerated	Benign
	RARA	G248D	0.53	17	38,508,695	38,508,695	G	A	Damaging	Probably damaging
	SOX9	T316A	0.44	17	70,119,944	70,119,944	A	A	Tolerated	Benign
	SESN1	H47R	0.48	6	109,415,137	109,415,137	T	C	Tolerated	Benign
	SETD2	G1649E	0.46	3	4,714,3017	47,143,017	C	T	Damaging	Probably damaging
	ANKRD11	A2284V	0.47	16	89346099	89,346,099	G	A	(not scored)	Benign
	TET3	V1137I	0.49	2	74,327,729	74,327,729	G	A	Tolerated	Benign
	ZFHX3	Q3203_Q3204del	0.28	16	72,822,564	72,822,569	TGCTGC	–	–	–

Mutational analysis of patient samples

Targeted sequencing for recurrent mutations was done by MSK-IMPACT [16] targeting all coding regions of 585 genes known to be recurrently mutated in leukemias, lymphomas, and solid tumors. Targeted next generation RNA sequencing platform (199-gene Archer panel) was also performed.

Cell culture and cytokine measurement

THP-1 (human acute monocytic leukemia cell line), HEK293T (cell line derived from human embryonic kidney 293 cells), and 32D (32Dcl3; murine myeloblast-like cell line) cells were cultured in IMDM/10% FCS (fetal calf serum, heat inactivated), DMEM/10% FCS, and IMDM/10% FCS + mIL3 (R&D Systems; 1 ng/mL), respectively. None of the cell lines above were listed in the database of commonly misidentified cell lines maintained by ICLAC and NCBI Biosample. For the cytokine/chemokine measurement, 1×10^6 THP-1 cells were cultured in a six-well plate and treated with phorbol 12-myristate 13-acetate (PMA; Millipore Sigma) at 10 ng/mL to induce differentiation into macrophage-like cells. The supernatant was collected at 72 h and the cytokine concentrations were measured using MILLIPLEX MAP Human Cytokine/Chemokine Magnetic Bead Panel (Millipore) by following instruction provided by the manufacturer. Standard curves were analyzed using Millipore Milliplex Analyst 5.1 Software.

Retroviral transduction and serial replating assays

BM cells from 5-fluoruracil (150 mg/kg) treated C57BL/6 mice were extracted as previously described [17]. RBCs were removed by ACK lysis buffer, and nucleated BM cells were transduced with viral supernatants containing MSCV-RUNX1$^{WT/G60C}$-IRES-GFP, MSCV-RUNX1/RUNX1T1-IRES-GFP, or MSCV-MEK2$^{WT/P128L}$-IRES-GFP for 2 days in RPMI/20% FCS supplemented with mouse stem cell factor (mSCF; 25 ng/mL; R&D Systems), mouse IL-3 (mIL3; 10 ng/mL; R&D Systems), and mIL-6 (10 ng/mL; R&D Systems). GFP-sorted cells were used for the following serial replating assays as described [17]. Briefly, single-cell suspension was prepared and 15,000 cells/1.5 mL were plated in triplicate in cytokine supplemented methylcellulose medium (MethoCult^{TM} GF M3434; StemCell Technologies), and colonies were enumerated weekly.

Reporter assay

Analysis of luciferase activity was performed as described previously [18]. Cells were transfected with a M-CSF receptor (M-CSFR) [19] plasmid (and expression vectors for RUNX1^{WT} and RUNX1^{G60C}) using Polyethylenimine (Polysciences, Inc.). Transfected cells were harvested 48 h later and assayed for luciferase activity with a dual luciferase kit (Promega). Firefly luciferase activity was measured as relative light units. Relative light units from individual transfection were normalized by measurement of Renilla luciferase activity in the same samples. Relative M-CSFR promoter activity was presented as the ratio of normalized luciferase activity of empty vector-transduced cells.

Histological analyses

BM biopsies from the patients were decalcified and fixed in 4% paraformaldehyde, dehydrated, and embedded in paraffin. Paraffin blocks were sectioned at 4 μm and stained with hematoxylin and eosin. Immunohistochemical staining was performed using anti-phosphor-ERK antibody (clone

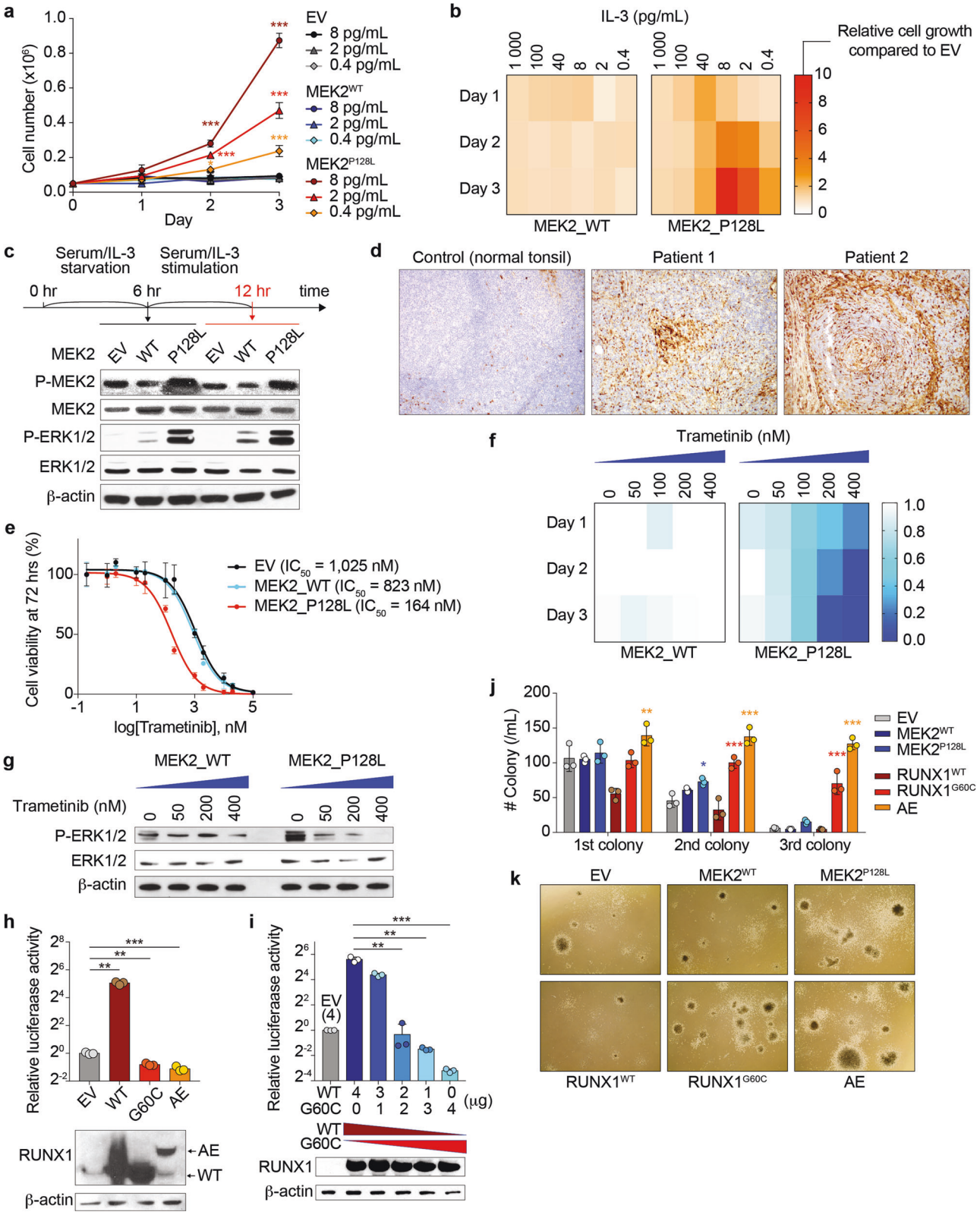
a
Cell number (x10^6)
Day
EV
8 pg/mL
2 pg/mL
0.4 pg/mL
MEK2WT
MEK2P128L
b
IL-3 (pg/mL)
Relative cell growth compared to EV
Day 1
Day 2
Day 3
MEK2_WT
MEK2_P128L
c
Serum/IL-3 starvation
Serum/IL-3 stimulation
0 hr
6 hr
12 hr
time
MEK2
P-MEK2
P-ERK1/2
ERK1/2
β-actin
d
Control (normal tonsil)
Patient 1
Patient 2
e
Cell viability at 72 hrs (%)
log[Trametinib], nM
EV (IC50 = 1,025 nM)
MEK2_WT (IC50 = 823 nM)
MEK2_P128L (IC50 = 164 nM)
f
Trametinib (nM)
g
Trametinib (nM)
h
Relative luciferase activity
RUNX1
AE
WT
β-actin
i
Relative luciferase activity
WT
G60C
RUNX1
β-actin
j
Colony (/mL)
1st colony
2nd colony
3rd colony
EV
MEK2WT
MEK2P128L
RUNX1WT
RUNX1G60C
AE
k
EV
MEK2WT
MEK2P128L
RUNX1WT
RUNX1G60C
AE

◀ **Fig. 2 Pathogenic roles of mutant MEK2 and mutant RUNX1. a**, **b** Cell growth of isogenic 32D cells cultured with various concentration of mouse IL-3 (**a**). Heatmaps were made based on relative cell growth of $MEK2^{WT}$ and $MEK2^{P128L}$ expressing cells compared with EV (empty vector)-transduced cells in **b** ($n = 3$ per genotype; the mean percentage ± standard deviation (SD); two-way ANOVA with Dunnett's multiple comparison test). **c** Representative western blot (WB) analysis of isogenic 32D cells from three biologically independent experiments with similar results. Experimental design is shown above. **d** Representative immunohistochemistry of phospho-ERK1/2 for the lymph nodes from both patients 1 and 2 as well as a normal tonsil as a control (original magnification ×100). **e** Dose response curves of isogenic 32D cells to Trametinib ($n = 3$; the mean value ± SD is shown). IC_{50} value for each genotype is indicated. **f** Cell growth of isogenic 32D cells cultured with various concentration of Trametinib. Heatmaps were made based on relative cell growth of $MEK2^{WT}$ and $MEK2^{P128L}$ expressing cells compared with EV (empty vector)-transduced cells in Supplementary Fig. 2c–e. **g** Representative WB analysis of isogenic 32D cells from three biologically independent experiments with similar results. **h** Luciferase activity of isogenic THP-1 cells retrovirally transduced with indicated constructs (top) and representative WB analysis of the same cells using an antibody against RUNX1 which recognizes N-terminus of RUNX1 protein (bottom). These cells were transfected with a M-CSF receptor reporter plasmid, and luciferase activities were measured as previously described [18] and presented as the fold change relative to EV-transduced cells (AE: RUNX1/RUNX1T1 (AML1/ETO); $n = 3$; the mean + SD; one-way ANOVA followed by Holm-Sidek's multiple comparison test). **i** Luciferase activity of HEK293T cells transfected with the reporter plasmid and mammalian expression vectors for $RUNX1^{WT}$ and $RUNX1^{G60C}$ at various doses as indicated (data are shown as in **h**). **j**, **k** Results of serial replating assays using primary mouse BM cells transduced with indicated constructs ($n = 3$ per genotype). Number of colonies (**j**) (the mean ± SD; two-way ANOVA with Tukey's multiple comparison test; p values compared with EV-expressing cells are shown), and representative images of colonies (**k**) (original magnification ×20) are shown. *$p < 0.05$; **$p < 0.01$; ***$p < 0.001$.

D13.14.4E, Cell signaling Technology). Images were acquired using an Olympus microscope.

RNA in situ mutation detection (BaseScope) assay

RNA in situ hybridization experiments were performed using RNAscope®, an RNA in situ hybridization technique described previously [20, 21]. Paired double-Z oligonucleotide probes were designed against target RNA using custom software. The following probes were used: I-BA-Hs-MAP2K2-P128L-Cand1, cat no. 720821, NM_030662.3, 1zz pair, nt 610–643; I-BA-Hs-MAP2K2-P128WT-Cand1, cat no. 720841, NM_030662.3, 1zz pair, nt 611–642. The BaseScope™ Reagent Kit (Advanced Cell Diagnostics, Newark, CA) was used according to the manufacturer's instructions. FFPE cell and tissue sections were prepared according to manufacturer's recommendations. Each sample was quality controlled for RNA integrity with a 1zz probe specific to the housekeeping gene PPIB. Negative control background staining was evaluated using a 1zz probe specific to the bacterial dapB gene.

Antibodies and reagents

For western blotting, the following antibodies were used: Phospho-MEK1/2 (Ser217/221) (Cell Signaling Technologies; #9154S), MEK1/2 (Cell Signaling Technologies; #9126S), Phospho-p44/42 MAPK (Erk1/2) (thr202/Tyr204) (Cell Signaling Technologies; #4370S), p44/42 MAPK (Erk1/2) (Cell Signaling Technologies; #4695S), β-actin (Sigma-Aldrich; A-5441). Trametinib (GSK1120212) (S2673), Selumetinib (AZD6244) (S1008), and U0126-EtOH (S1102) were perchased from Selleckchem.

Statistics and reproducibility

Statistical significance was determined by (1) unpaired two-sided Student's t-test after testing for normal distribution, (2) one-way or two-way ANOVA followed by Tukey's, Holm-Sidak's, or Dunnett's multiple comparison test, or (3) Kruskal-Wallis tests with Uncorrected Dunn's test where multiple comparisons should be adjusted. Representative WB results are shown from three or more than three biologically independent experiments.

Data availability

The data that support the findings of this study are available from the corresponding author upon reasonable request. Sequencing data have been deposited in NCBI ClinVar under accession number SCV000965590-SCV000965596. Other data that support this study's findings are available from the authors upon reasonable request.

Acknowledgements This study was funded in part through the NIH/NCI Cancer Center Support Grant P30 CA008748. AY is a Special Fellow of The Leukemia and Lymphoma Society and supported by grants from the Aplastic Anemia and MDS International Foundation (AA&MDSIF), the Lauri Strauss Leukemia Foundation, the Leukemia and Lymphoma Society Special Fellow Award, and JSPS Overseas Research Fellowships. OA-W is supported by grants from NIH/NHLBI (R01 HL128239), the Department of Defense Bone Marrow Failure Research Program (W81XWH-16-1-0059), the Starr Foundation (I8-A8-075), the Henry & Marilyn Taub Foundation, the Edward P. Evans Foundation, the Josie Robertson Investigator Program, the Leukemia and Lymphoma Society, and the Pershing Square Sohn Cancer Research Alliance. WX is supported by a grant from Castleman's Awareness and Research Effort/Castleman Disease Collaborative Network.

Author contributions AY, OA-W, and WX designed the study; AY, AVP, MEA, and HH performed experiments; TMT, NZ, and XC provided clinical samples; JP, JB, AS, DCF, and AD coordinated the project; AY, OA-W, and WX prepared the paper with help from all co-authors.

Compliance with ethical standards

Conflict of interest DCF receives research funding from EUSA Pharma for the ACCELERATE Registry (formerly sponsored by

Janssen Pharmaceuticals). AD has received personal fees from Roche, Corvus Pharmaceuticals, Physicians' Education Resource, Seattle Genetics, Peerview Institute, Oncology Specialty Group, Pharmacyclics, Celgene, and Novartis and research grants from National Cancer Institute, Roche. OA-W has served as a consultant for H3 Biomedicine, Foundation Medicine Inc., Merck, and Janssen and serves on the scientific advisory board of Envisagenics Inc.; OA-W has received personal speaking fees from Daiichi Sankyo. OA-W has received prior research funding from H3 Biomedicine unrelated to the current paper. OA-W is an inventor on a provisional patent application submitted by Fred Hutchinson Cancer Research Center that covers BRD9 activation in cancer. WX has received research support from Stemline therapeutics. Other authors have nothing to disclose.

References

1. Kawabata H, Takai K, Kojima M, Nakamura N, Aoki S, Nakamura S, et al. Castleman-Kojima disease (TAFRO syndrome): a novel systemic inflammatory disease characterized by a constellation of symptoms, namely, thrombocytopenia, ascites (anasarca), microcytic anemia, myelofibrosis, renal dysfunction, and organomegaly: a status report and summary of Fukushima (6 June, 2012) and Nagoya meetings (22 September, 2012). J Clin Exp Hematop. 2013;53:57–61.
2. Inoue M, Ankou M, Hua J, Iwaki Y, Hagihara M, Ota Y. Complete resolution of TAFRO syndrome (thrombocytopenia, anasarca, fever, reticulin fibrosis and organomegaly) after immunosuppressive therapies using corticosteroids and cyclosporin A: a case report. J Clin Exp Hematop. 2013;53:95–9.
3. Iwaki N, Fajgenbaum DC, Nabel CS, Gion Y, Kondo E, Kawano M, et al. Clinicopathologic analysis of TAFRO syndrome demonstrates a distinct subtype of HHV-8-negative multicentric Castleman disease. Am J Hematol. 2016;91:220–6.
4. Iwaki N, Gion Y, Kondo E, Kawano M, Masunari T, Moro H, et al. Elevated serum interferon gamma-induced protein 10 kDa is associated with TAFRO syndrome. Sci Rep. 2017;7:42316.
5. Pierson SK, Stonestrom AJ, Shilling D, Ruth J, Nabel CS, Singh A, et al. Plasma proteomics identifies a 'chemokine storm' in idiopathic multicentric Castleman disease. Am J Hematol. 2018;93:902–12.
6. Liu AY, Nabel CS, Finkelman BS, Ruth JR, Kurzrock R, van Rhee F, et al. Idiopathic multicentric Castleman's disease: a systematic literature review. Lancet Haematol. 2016;3:e163–75.
7. Fajgenbaum DC, Uldrick TS, Bagg A, Frank D, Wu D, Srkalovic G, et al. International, evidence-based consensus diagnostic criteria for HHV-8–negative/idiopathic multicentric Castleman disease. Blood. 2017;129:1646–57.
8. Ozkaya N, Rosenblum MK, Durham BH, Pichardo JD, Abdel-Wahab O, Hameed MR, et al. The histopathology of Erdheim-Chester disease: a comprehensive review of a molecularly characterized cohort. Mod Pathol. 2018;31:581–97.
9. Song WJ, Sullivan MG, Legare RD, Hutchings S, Tan X, Kufrin D, et al. Haploinsufficiency of CBFA2 causes familial thrombocytopenia with propensity to develop acute myelogenous leukaemia. Nat Genet. 1999;23:166–75.
10. Yoshimi A, Toya T, Nannya Y, Takaoka K, Kirito K, Ito E, et al. Spectrum of clinical and genetic features of patients with inherited platelet disorder with suspected predisposition to hematological malignancies: a nationwide survey in Japan. Ann Oncol. 2016;27:887–95.
11. Nagy A, Bhaduri A, Shahmarvand N, Shahryari J, Zehnder JL, Warnke RA, et al. Next-generation sequencing of idiopathic multicentric and unicentric Castleman disease and follicular dendritic cell sarcomas. Blood Adv. 2018;2:481–91.
12. Abelson S, Collord G, Ng SWK, Weissbrod O, Mendelson Cohen N, Niemeyer E, et al. Prediction of acute myeloid leukaemia risk in healthy individuals. Nature. 2018;559:400–4.
13. Jaiswal S, Fontanillas P, Flannick J, Manning A, Grauman PV, Mar BG, et al. Age-related clonal hematopoiesis associated with adverse outcomes. N Engl J Med. 2014;371:2488–98.
14. Baker TS, Gambino KJ, Schriefer L, Lim JY, Steinberg KM, Fajgenbaum DC, et al. A novel FAS mutation with variable expressivity in a family with unicentric and idiopathic multicentric Castleman disease. Blood Adv. 2018;2:2959–63.
15. Bolze A, Byun M, McDonald D, Morgan NV, Abhyankar A, Premkumar L, et al. Whole-exome-sequencing-based discovery of human FADD deficiency. Am J Hum Genet. 2010;87:873–81.
16. Cheng DT, Mitchell TN, Zehir A, Shah RH, Benayed R, Syed A, et al. Memorial sloan kettering-integrated mutation profiling of actionable cancer targets (MSK-IMPACT): a hybridization capture-based next-generation sequencing clinical assay for solid tumor molecular oncology. J Mol Diagn. 2015;17:251–64.
17. Yoshimi A, Lin KT, Wiseman DH, Rahman MA, Pastore A, Wang B, et al. Coordinated alterations in RNA splicing and epigenetic regulation drive leukaemogenesis. Nature. 2019;574:273–7.
18. Yoshimi A, Goyama S, Watanabe-Okochi N, Yoshiki Y, Nannya Y, Nitta E, et al. Evi1 represses PTEN expression and activates PI3K/AKT/mTOR via interactions with polycomb proteins. Blood. 2011;117:3617–28.
19. Michaud J, Wu F, Osato M, Cottles GM, Yanagida M, Asou N, et al. In vitro analyses of known and novel RUNX1/AML1 mutations in dominant familial platelet disorder with predisposition to acute myelogenous leukemia: implications for mechanisms of pathogenesis. Blood. 2002;99:1364–72.
20. Wang F, Flanagan J, Su N, Wang LC, Bui S, Nielson A, et al. RNAscope: a novel in situ RNA analysis platform for formalin-fixed, paraffin-embedded tissues. J Mol Diagn. 2012;14:22–9.
21. Li Z, Lan X, Li C, Zhang Y, Wang Y, Xue W, et al. Recurrent PDGFRB mutations in unicentric Castleman disease. Leukemia. 2019;33:1035–8.